1-1-2012

Effects of initial static shear on liquefaction and large deformation properties of loose saturated Toyoura sand in undrained cyclic torsional shear tests

Gabriele Chiaro
University of Wollongong, gchiaro@uow.edu.au

Junichi Koseki
IIS, University of Tokyo, koseki@iis.u-tokyo.ac.jp

Takeshi Sato
Integrated Geotechnology Institute Ltd, tsato@iis.u-tokyo.ac.jp

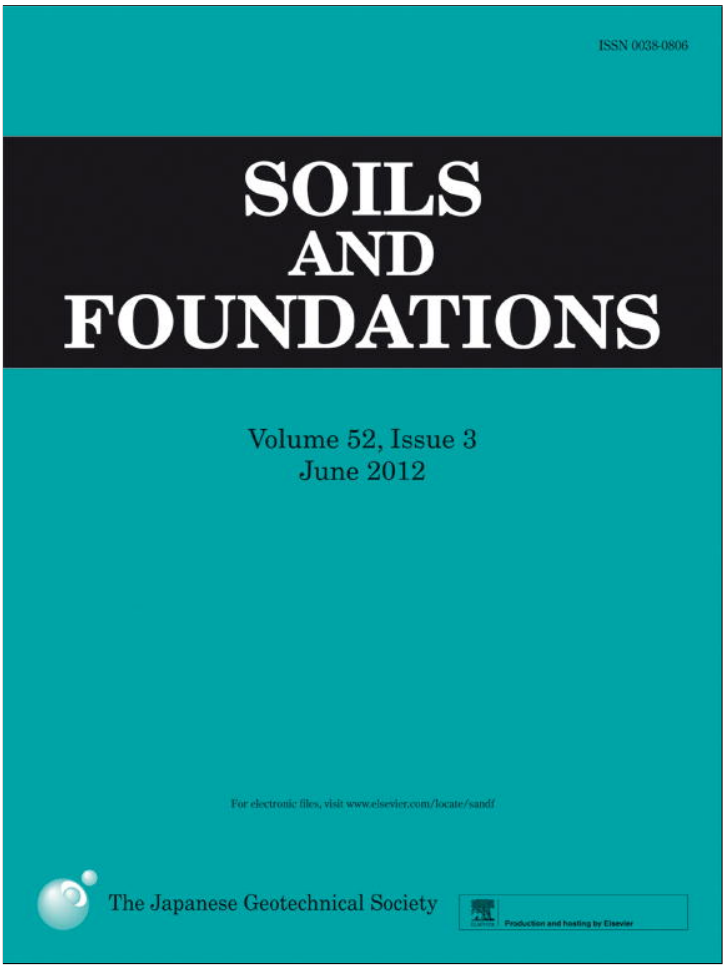

Soils and Foundations 2012;52(3):498–510

The Japanese Geotechnical Society

Soils and Foundations

www.sciencedirect.com
journal homepage: www.elsevier.com/locate/sandf

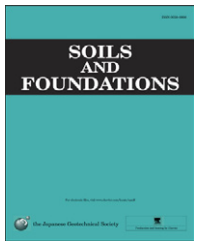

Effects of initial static shear on liquefaction and large deformation properties of loose saturated Toyoura sand in undrained cyclic torsional shear tests

Gabriele Chiaro[a,b], Junichi Koseki[c,*], Takeshi Sato[d]

[a]*Centre for Geomechanics and Railway Engineering, University of Wollongong, Australia*
[b]*Department of Civil Engineering, University of Tokyo, Japan*
[c]*Institute of Industrial Science, University of Tokyo, Japan*
[d]*Integrated Geotechnology Institute Ltd., Japan*

Available online 15 June 2012

Abstract

This study focused on the role which static shear plays on the large deformation behavior of loose saturated sand during undrained cyclic loading. A series of undrained cyclic torsional shear tests was performed on saturated Toyoura sand specimens up to single amplitude shear strain exceeding 50%. Three types of cyclic loading patterns, i.e., stress reversal, intermediate and non-reversal, were employed by varying the initial static shear level and the cyclic shear stress amplitude. The observed types of failure could be distinguished into liquefaction (cyclic and rapid flow) and residual deformation by comparing both monotonic and cyclic undrained behavior. It was found that the presence of initial static shear does not always lead to an increase in the resistance to liquefaction or strain accumulation; they could either increase or decrease with an increasing initial static shear level depending on the type of loading pattern and failure behavior. In addition, according to the failure behavior which the specimens exhibited, three modes of development of large residual deformation were observed.

Keywords: Large strain; Liquefaction; Static shear stress; Torsional shear tests; Undrained cyclic behavior

Introduction

Slope failure is one of the most serious geotechnical disasters brought about by earthquakes that may cause substantial economical losses as well as a great number of human losses. Yet, its mechanism is not well understood. In particular, the catastrophic liquefaction-induced failure behavior of natural and artificial slopes of sandy deposits and the consequent development of extremely large ground deformation are both poorly understood.

Past large-magnitude earthquakes (e.g., the 1964 Niigata Earthquake and the 1983 Nihonkai-Chubu Earthquake in Japan) have indicated that extremely large horizontal ground deformation can occur in liquefied sandy deposits in coastal or river areas. When lateral spreading and/or flow slides take place, ground displacement may exceed several meters, even in gentle slopes with an inclination of less than a few percent, resulting in severe damage to

*Corresponding author.
E-mail addresses: gchiaro@uow.edu.au (G. Chiaro), koseki@iis.u-tokyo.ac.jp (J. Koseki), sato@iis.u-tokyo.ac.jp (T. Sato).
Peer review under responsibility of The Japanese Geotechnical Society.

Production and hosting by Elsevier

0038-0806
http://dx.doi.org/10.1016/j.sandf.2012.05.008

buildings, infrastructures and lifeline facilities (Hamada et al., 1994).

It is recognized that the behavior of soil elements within a sloped ground composed of saturated sands is different from that of a level ground during cyclic loading. This is because the soil elements are subjected to an initial static shear stress on the horizontal plane or an assumed failure surface. During earthquake shaking, these elements are subjected to additional cyclic shear stress due to shear waves propagating vertically upward from the bedrock. The superimposition of static and cyclic shear stress can have a major effect on the response of the soil, leading to liquefaction and the development of extremely large ground deformation.

Various studies have focused on the effects of static shear on the undrained cyclic triaxial behavior of sand. Lee and Seed (1967) and Seed (1968) found that the larger the ratio of initial static shear stress to initial confining pressure acting on a horizontal plane, the greater the horizontal cyclic shear stress required to induce liquefaction in a given number of stress cycles. Furthermore, Vaid and Chern (1983) showed that the cyclic strength can either increase or decrease due to the presence of static shear stress and depending on the difference in density of the specimens, the magnitude of the static shear and the definition of liquefaction resistance. In particular, for loose sand with higher initial static shear, the cyclic strength was reduced due to flow deformation. Based on the difference in the effective stress paths and the stress–strain relationships, Hyodo et al. (1991) classified the undrained cyclic behavior of anisotropically consolidated specimens into three types, i.e., stress reversal, non-reversal and intermediate. They observed that in the stress reversal and intermediate cases on loose samples, failure could be associated with liquefaction, while in the non-reversal case, residual deformation brought the sample to failure even though no liquefaction had occurred. Failure was not observed in the non-reversal case on dense specimens. Recent work by Yang and Sze (2011) involved an investigation of the interdependence of major factors affecting the liquefaction behavior of sand, such as relative density, confining pressure and static shear. Clearly, the initial static shear stress has a significant effect on the liquefaction resistance, which is dependent on the initial relative density and the confining pressure. In addition, there are three different failure modes for sand under undrained triaxial cyclic loadings, namely, flow-type failure, cyclic mobility and accumulated plastic strain. Among these, the flow-type failure is the most critical, since it is characterized by abrupt, runaway deformations with no warning signals.

It is recognized that simple shear tests simulate field stress conditions expected during earthquakes more accurately than triaxial tests. The conclusions achieved by Yoshimi and Oh-oka (1975), through the performance of ring shear tests, were substantially opposite to those based on the triaxial tests by Lee and Seed (1967) and Seed (1968). They pointed out that to induce liquefaction and the development of large cyclic shear strain, the reversal of shear stress is necessary. Vaid and Finn (1979) evaluated the cyclic loading behavior of Ottawa sand under plane strain conditions using a simple shear device. They clarified that, in general, the resistance to liquefaction can either increase or decrease due to the presence of static shear and depending on the relative density of the specimens, the magnitude of the initial static shear stress and the shear strain level of interest. Tatsuoka et al. (1982) investigated the stress–strain behavior of sand under torsional simple shear conditions, including the case with static shear. Their results were well in accordance with those reported by Vaid and Finn (1979), confirming that a torsional simple shear apparatus could be employed as a very useful tool for evaluating the cyclic undrained stress–strain behavior of sand.

However, it should be noted that in all of the above studies, the shear strain levels employed were limited to the range of 10–20%. This is due mainly to the mechanical limitations of the employed apparatus and/or the large extent of the non-uniform deformation of the specimen at higher strain levels, as well as the technical difficulties involved with correcting the effects of the membrane force during the tests.

Therefore, it is not possible to fully describe the occurrence of a liquefaction-induced ground deformation of several meters, which means that ground strain may reach over 100% on a slightly sloped ground.

Based on the above-mentioned background, the aim of this study is to better understand the role which static shear plays on the large deformation behavior of loose saturated sand during undrained cyclic loading. In this paper, the results of investigations on the effects of the initial static shear on the undrained cyclic behavior of saturated Toyoura sand specimens, subjected to cyclic torsional shear loading up to single amplitude of about 50% under various combinations of static and subsequent cyclic shear, are presented.

Test apparatus

To reach extremely large torsional shear displacements, a fully automated torque-loading apparatus on hollow cylindrical specimens (Fig. 1), developed by Koseki et al. (2007) and Kiyota et al. (2008), was employed. It is capable of achieving double-amplitude torsional shear strain levels exceeding 100% by using a belt-driven torsional loading system that is connected to an AC servo motor through electro-magnetic clutches and a series of reduction gears.

A two-component load cell, which is installed inside the pressure cell, as shown in Fig. 1(a), having torque and axial load capacities of 0.15 kNm and 8 kN, respectively, was used to measure both the torque and the axial load components. The confining pressure, obtained by the difference in pressure levels between the cell pressure and the pore water pressure, was measured by a high-capacity differential pressure transducer (HCDPT) with a capacity of over 600 kPa. To evaluate

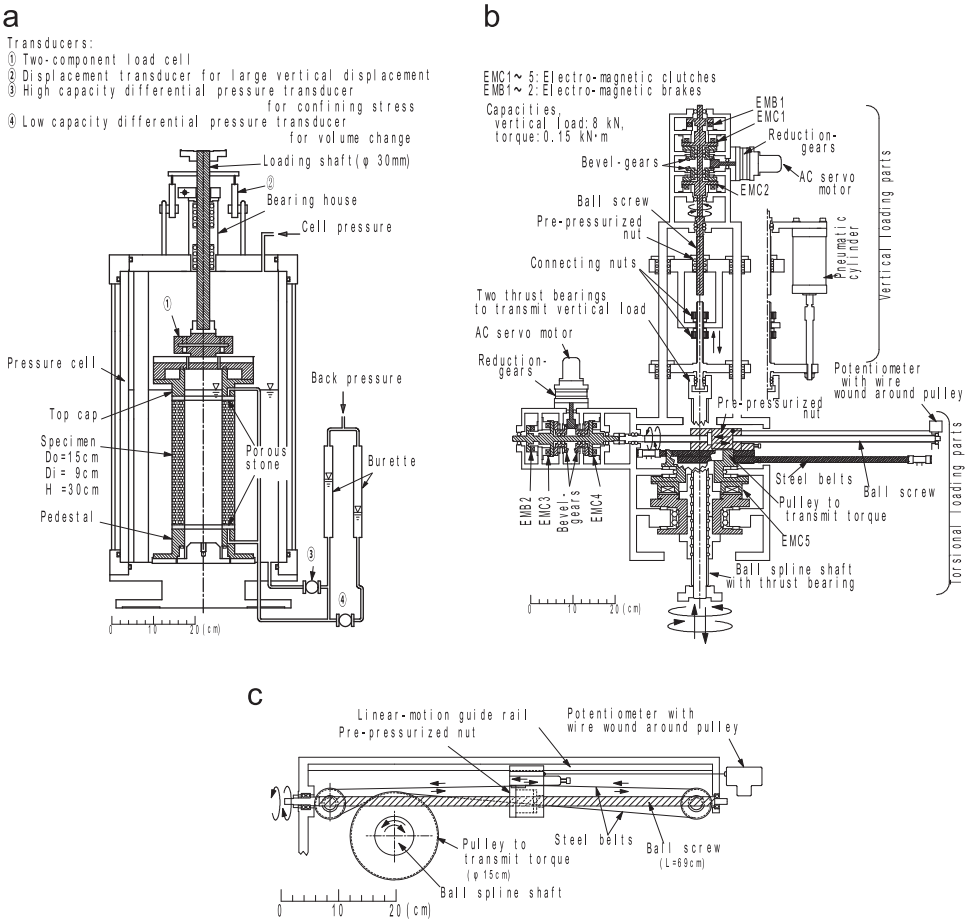

Fig. 1. (a) Torsional shear test apparatus on hollow cylindrical specimen, (b) loading device, and (c) plan view of torque-transmission part (after Kiyota et al., 2008).

large torsional deformations, a potentiometer with a wire and a pulley was employed (Fig. 1(b) and (c)).

To conduct the cyclic shear tests, the specified shear stress amplitude was controlled by a computer, which monitors the outputs from the load cell, computes the shear stress (i.e., the measured shear stress was corrected for the effects of the membrane force, as described by Koseki et al., 2005) and controls the device accordingly.

Material, specimen preparation and testing procedures

All the tests were performed on Toyoura sand, which is uniform sand with a negligible fines content under 75 μm (specific gravity $G_S=2.656$, maximum void ratio $e_{max}=0.992$, minimum void ratio $e_{min}=0.632$, mean diameter $D_{50}=0.16$ mm and fines content $F_C=0.1\%$). Several specimens with a relative density in the range of 44–48% (i.e., void ratio $e=0.833$–0.819) were prepared by the air pluviation method. To minimize the degree of inherent anisotropy in the radial direction of the hollow cylindrical sand specimens, the sample preparation was carried out carefully by pouring the air-dried sand particles into a mold, while moving the nozzle of the pluviator radially and circumferentially at the same time in alternative directions, i.e., first in a clockwise direction and then in a counter-clockwise direction (De Silva et al., 2006). In addition, to obtain specimens of highly uniform density, the falling height was kept constant throughout the pluviation process.

In order to get a high degree of saturation, the double vacuum method (Ampadu and Tatsuoka, 1993) was employed; de-aired water was circulated into the specimens and a back pressure of 200 kPa was applied. Skempton's *B*-values of more than 0.96 were observed in all the specimens used in the tests.

The hollow cylindrical specimens, with initial dimensions of 150 mm in outer diameter, 90 mm in inner diameter and 300 mm in height, were isotropically consolidated by increasing the effective stress state up to 100 kPa. They were then monotonically sheared in order to apply a specified value of initial static shear representative of the sloping ground conditions, at a strain rate of 0.5%/min, while keeping drained conditions. After applying a drained creep loading for 5 min or even longer, in order to study the behavior of the sandy specimens under seismic conditions (i.e., liquefaction resistance and/or the development of large deformation), undrained cyclic torsional loading with a constant amplitude of shear stress was applied at a constant shear strain rate of about 2.5%/min.

Table 1
Test conditions.

Test	e	Dr	τ_{cyclic}	τ_{static}	τ_{max}	τ_{min}	Loading pattern
1	0.825	46.4	16	0	+16	−16	Reversal
2	0.828	45.5	16	5	+21	−11	Reversal
3	0.824	46.6	16	10	+26	−6	Reversal
4	0.833	44.2	16	15	+31	−1	Reversal
5	0.825	46.5	16	16	+32	0	Intermediate
6	0.820	47.9	16	17	+33	+1	Non-reversal
7	0.829	45.3	16	20	+36	+4	Non-reversal
8	0.819	48.1	20	0	+20	−20	Reversal
9	0.819	48.0	20	5	+25	−15	Reversal
10	0.828	45.6	20	10	+30	−10	Reversal
11	0.832	44.4	20	15	+35	−5	Reversal
12	0.823	46.9	20	20	+40	0	Intermediate
13	0.826	46.1	20	25	+45	5	Non-reversal

e: void ratio, Dr: relative density (%) measured at an isotropic stress state of $\sigma'_c = 100$ kPa,
τ_{cyclic}: cyclic shear stress (kPa), τ_{static}: initial static shear stress (kPa),
$\tau_{max} = \tau_{static} + \tau_{cyclic}$: maximum combined shear stress (kPa),
$\tau_{min} = \tau_{static} - \tau_{cyclic}$: minimum combined shear stress (kPa).

As listed in Table 1, cyclic loading tests were performed over a wide range of initial static shear, varying from 0 to 25 kPa. Two levels of cyclic shear stress amplitude, 16 kPa and 20 kPa, were employed in this study in order to consider various combinations of initial static and cyclic shear stress. The loading direction was reversed when the amplitude of the combined shear stress, which was corrected for the effect of the membrane force, reached the target value. During the process of the undrained cyclic torsional loading, the vertical displacement of the top cap was not allowed, with the aim to simulate as much as possible the simple shear condition that a ground undergoes during horizontal excitation.

It should be noted that the effects of the membrane penetration (MP), due to the excess pore water pressure generation, on the liquefaction resistance, was not considered in this study, since their extents would be independent of the drained static shear applied.

Reversal, intermediate and non-reversal cyclic loading patterns

The soil elements within a sloped ground are subjected to an initial static shear stress on the horizontal plane. During earthquake shaking, these elements can experience partially reversed or non-reversed shear stress loading conditions, due to the superimposition of the static shear stress with the cyclic shear stress. While referring to Hyodo et al. (1991), three types of cyclic loading patterns were employed in this study, i.e., stress reversal, intermediate and non-reversal, as schematically shown in Fig. 2. During each cycle of loading in some tests, the combined shear stress value was reversed from positive ($\tau_{max} = \tau_{static} + \tau_{cyclic} > 0$) to negative ($\tau_{min} = \tau_{static} - \tau_{cyclic} < 0$), or vice versa. This type of loading is hereafter called reversal loading (Fig. 2(a)), whereas the type of loading in which the reversal of the loading direction was made when the value of the combined shear stress achieved zero ($\tau_{min} = 0$) during the undrained torsional shear loading is called intermediate loading (Fig. 2(b)) and the type of loading in which the combined shear stress was always kept positive is called non-reversal loading (Fig. 2(c)).

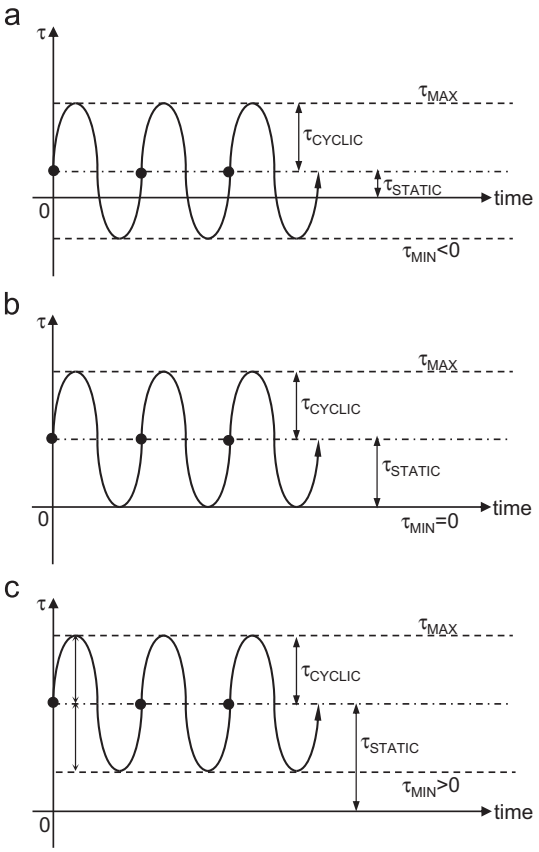

Fig. 2. Scheme of cyclic torsional shear loadings (adapted from Hyodo et al., 1991).

Tests results

Correction of torsional shear stress for membrane force

In performing torsional shear tests on hollow cylindrical specimens, the effect of the membrane force, brought about by the presence of inner and outer membranes, cannot be neglected (Koseki et al., 2007; among others). It becomes significantly important when the shear strain reaches an extremely high level (Kiyota et al., 2008). By employing the linear elasticity theory, which uses the Young's modulus of the membrane, the theoretical apparent shear stress (τ_m), induced by the inner and outer membranes, can be evaluated as follows:

$$\tau_m = \frac{t_m E_m (r_o^3 + r_i^3)\theta}{(r_o^3 - r_i^3)h} \quad (1)$$

where θ is the rotational angle of the top cap detected by the external potentiometer, h is the height of the specimen, r_o and r_i are the outer and inner radii of the specimen,

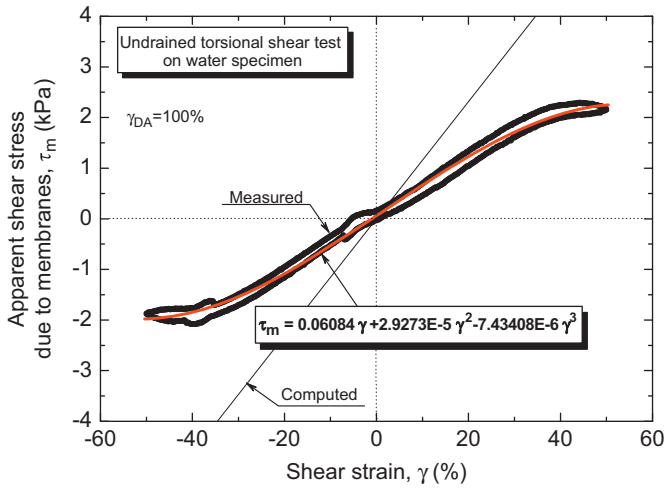

Fig. 3. Relationships between apparent shear stress due to membrane force and shear strain.

respectively, and t_m and E_m are the thickness (=0.3 mm) and the Young's modulus (=1492 kPa, after Koseki et al., 2005) of the membrane, respectively.

In order to confirm the validity of Eq. (1) in correcting for the effect of the membrane force, a special test was performed by pouring water between the inner and the outer membranes and shearing the water specimen cyclically under undrained conditions up to a double-amplitude shear strain of 100%. Fig. 3 shows both the experimental and the theoretical relationships between the shear strain and the apparent shear stress that are induced by the membranes due to the torsional deformation. The deviation of the actual membrane deformation from the uniform cylindrical one that is assumed in the theory became larger with an increase in the strain level. Hence, in this study, the shear stress was corrected for the effect of the membrane force by employing the polynomial approximation of the measured relationship between γ and τ_m, shown in Fig. 3.

Undrained cyclic torsional shear behavior of sand with static shear

As listed in Table 1, undrained cyclic tests were performed under reversal, intermediate and non-reversal loading patterns. The typical effective stress paths during cyclic loading for each type of loading pattern and the corresponding stress–strain relationships are presented in Figs. 4–6.

As shown in Fig. 4, in the case of reversal loading, cyclic mobility was observed in the effective stress path, where the effective stress recovered repeatedly after reaching the state of zero effective stress (i.e., full liquefaction). It was accompanied by a significant development of shear strain, as evidenced by the stress–strain relationship.

As shown in Fig. 5, in the case of intermediate loading, the behavior of the specimen was similar to that of the reversal case, in the sense that after achieving a fully

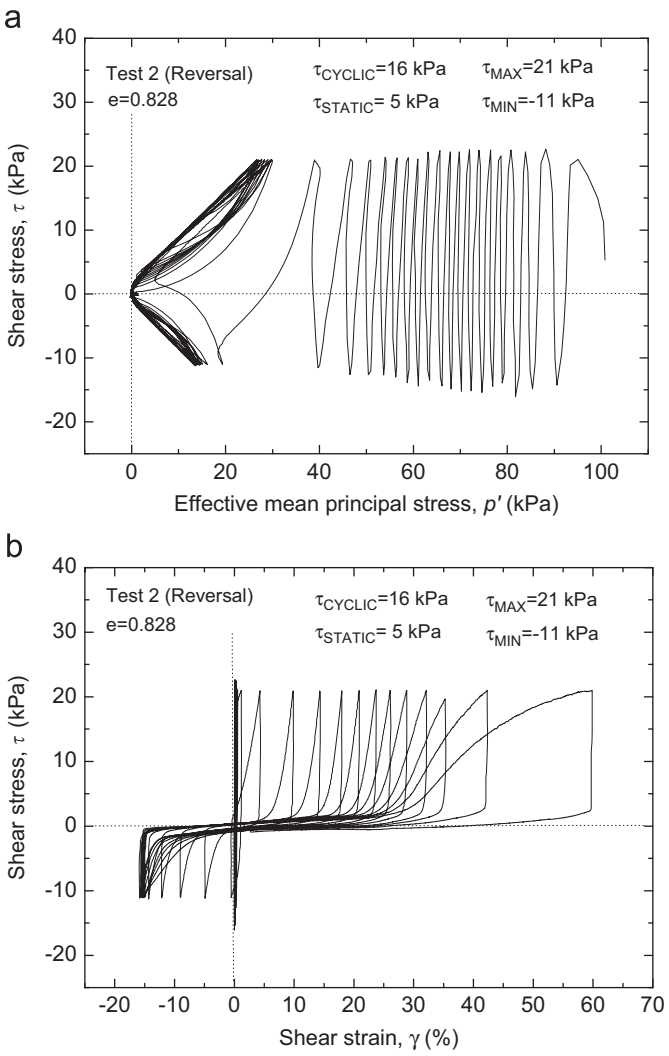

Fig. 4. Typical reversal undrained cyclic torsional shear test results.

liquefied state ($p'=0$), progressive large deformation developed while showing cyclic mobility.

Fig. 6 represents the case of non-reversal loading. The state of zero effective stress was not achieved even after applying 208 cycles of loading. Although liquefaction did not occur, a large shear strain exceeding 50% was reached, and the formation of a spiral shear band could be observed.

Undrained monotonic torsional shear behavior of sand with static shear

In Fig. 7, the effective stress paths and the stress–strain relationships during the first quarter cycle of undrained loading (i.e., equivalent to undrained monotonic loading) are shown for the three tests. The tests were conducted under almost the same initial conditions of void ratio and confining pressure by varying the initial static shear level.

All the specimens initially showed contractive behavior (i.e., a decrease in the p' value), during which the shear stress (τ) steadily increased to a transient peak (τ_{peak}). The

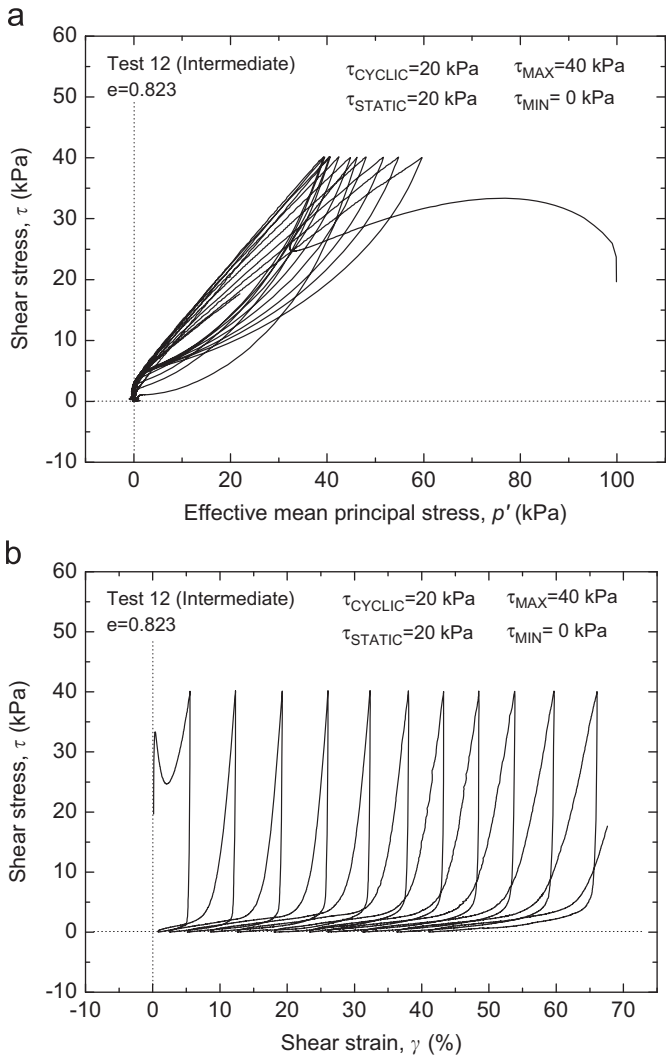

Fig. 5. Typical intermediate undrained cyclic torsional shear test results.

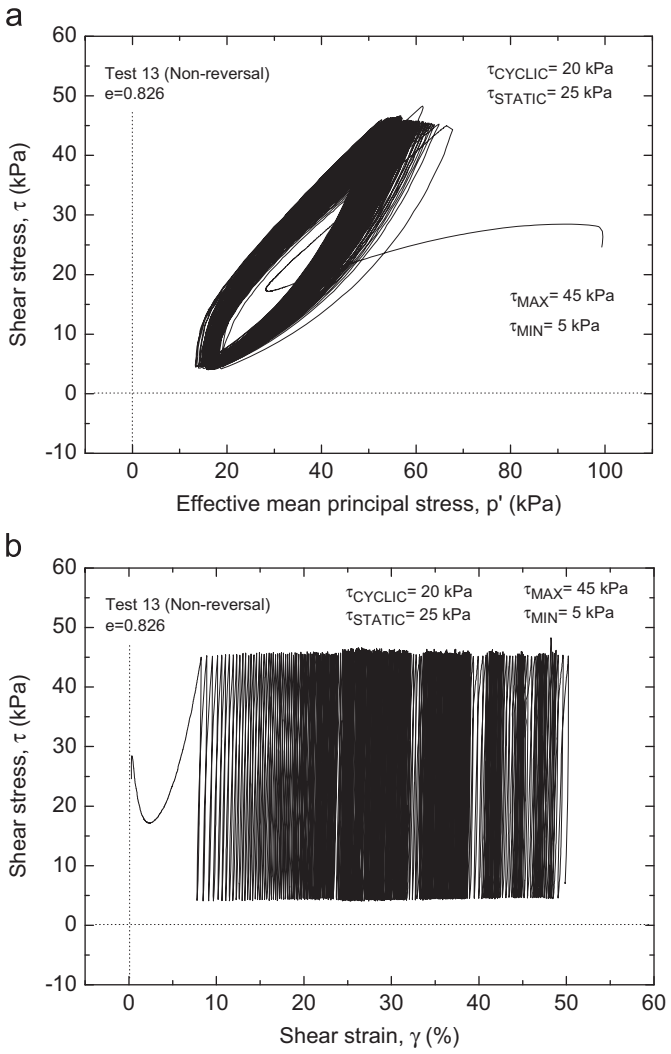

Fig. 6. Typical non-reversal undrained cyclic torsional shear test results.

peak points mark the initiation of unstable behavior, since the shear stress drops with further loading to a transient minimum value (or quasi steady state; Verdugo and Ishihara, 1996) during which the specimen deforms under nearly constant shear stress. As soon as the shear stress reaches the phase transformation line (PTL; Ishihara et al., 1975), dilative behavior takes place and the effective stress paths follow the failure envelope line.

Lade (1993) defined the instability line (IL) as the line that connects the peak points of the effective stress paths to the origin of the stress space. Furthermore, Kramer (1996) termed this line as the flow liquefaction surface (FLS), since flow liquefaction behavior was observed in the tests in which the monotonic or cyclic loading stress path exceeds the point of peak stress (τ_{peak}). They showed that the slope of this line can be uniquely determined for specimens having similar void ratios, irrespective of the initial effective stress level.

In the current study, it was found that under the same initial conditions of void ratio and confining pressure, the larger the initial static shear stress level, the greater the shear stress at the transient peak state (τ_{peak}). In addition, by drawing a line which connects the peak points, a boundary with similar features of the IL or FLS could be defined. In contrast to previous studies, this line does not pass through the origin of the stress space. However, flow liquefaction behavior was observed in the tests in which during the first quarter cycle of undrained loading the stress path exceeds the corresponding state of the transient peak stress (τ_{peak}), as was also observed by Kramer (1996).

Failure characteristics of sand with initial static shear by comparison of monotonic and cyclic undrained behaviors

A comparison between the undrained monotonic behavior and the cyclic behavior of sand was carried out by Vaid and Chern (1985) and Hyodo et al. (1994) using triaxial tests and by Alarcon-Guzman et al. (1988) using torsional shear tests. Vaid and Chern (1985) showed that in cyclic tests, flow deformation may be initiated when the stress path reaches the critical effective stress ratio line. On the other hand, Alarocn-Guzman et al. (1988) stated that flow deformation

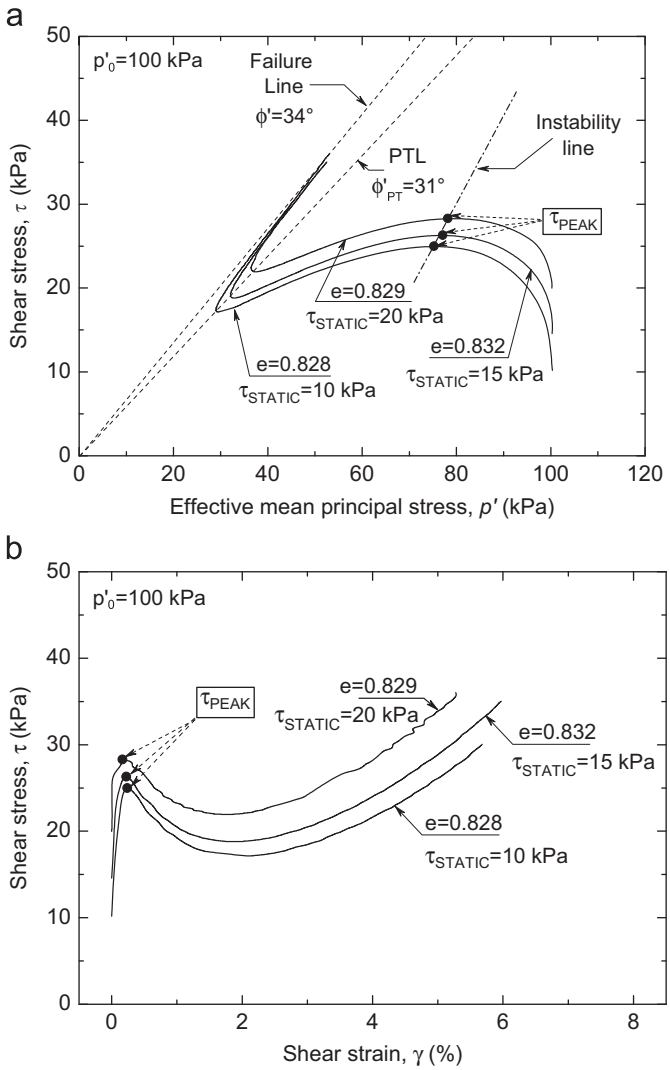

Fig. 7. Typical undrained monotonic torsional shear test results.

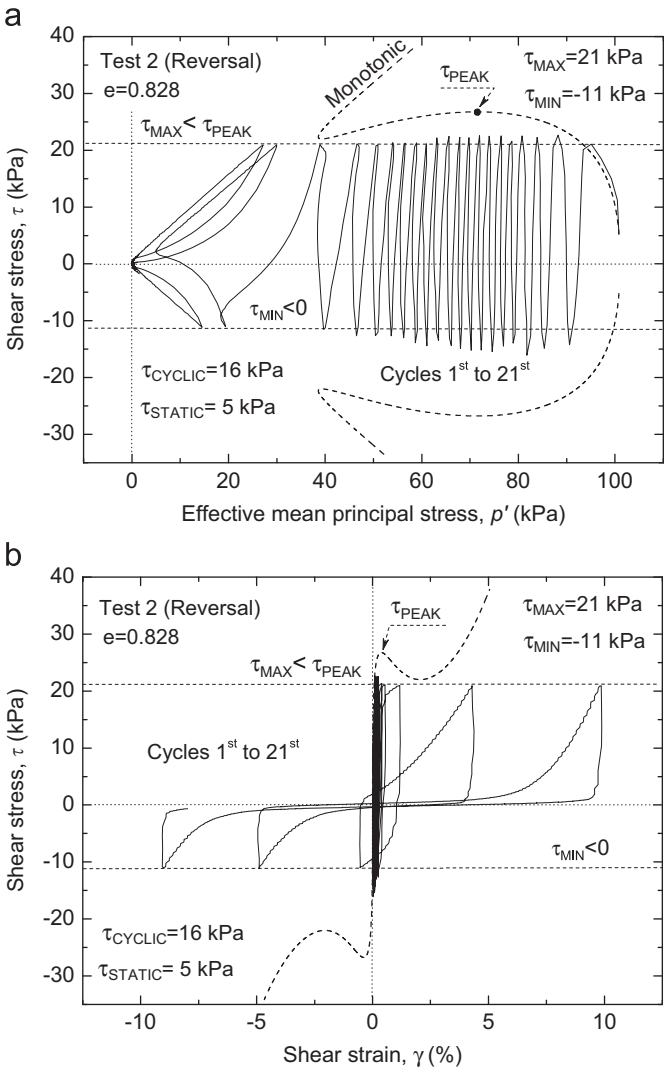

Fig. 8. Typical cyclic liquefaction behavior.

occurs during cyclic loading when the stress state reaches the effective path from monotonic tests. Moreover, Hyodo et al. (1994) found the occurrence of flow deformation to be triggered during cyclic loading when the stress state reaches the softening regions in the effective stress path from monotonic tests (i.e., the region between IL and PTL). However, these investigations did not clarify the effects of the initial static shear on the modes of failure (i.e., failure due to liquefaction or failure brought about by a large extent of deformation; Hyodo et al., 1991) of sand subjected to undrained cyclic loading, which were attempted herein.

In this study, the observed types of failure were distinguished into liquefaction and residual deformation based on the difference in the effective stress paths and the modes of development of the cyclic residual shear strain during both monotonic and cyclic loading behavior, as shown in Figs. 8–10.

Cyclic liquefaction

In some cyclic tests, as typically shown in Fig. 8, the shear stress reached a maximum value (τ_{max}), which was lower than the transient peak stress during undrained monotonic loading (τ_{peak}). In addition, the minimum shear stress value was negative ($\tau_{min} < 0$). Under these stress conditions (i.e., reversal stress), while undergoing several tens of cycles, due to the excess pore water pressure generation, the effective mean principal stress (p') progressively decreased and the stress state moved toward the failure envelope and finally reached the full liquefaction state ($p' = 0$). Then, in the post-liquefaction process, large deformations developed.

Rapid flow liquefaction

In other tests, as typically shown in Fig. 9, the shear stress reached a maximum value which was higher than the transient peak stress during undrained monotonic loading ($\tau_{max} > \tau_{peak}$), while the minimum shear stress value was negative ($\tau_{min} < 0$) or zero ($\tau_{min} = 0$) due to stress reversal or intermediate conditions, respectively. As a result, liquefaction took place, mostly in-between the first cycle of loading (few cycles for intermediate tests), and a rapid development of residual strain was observed.

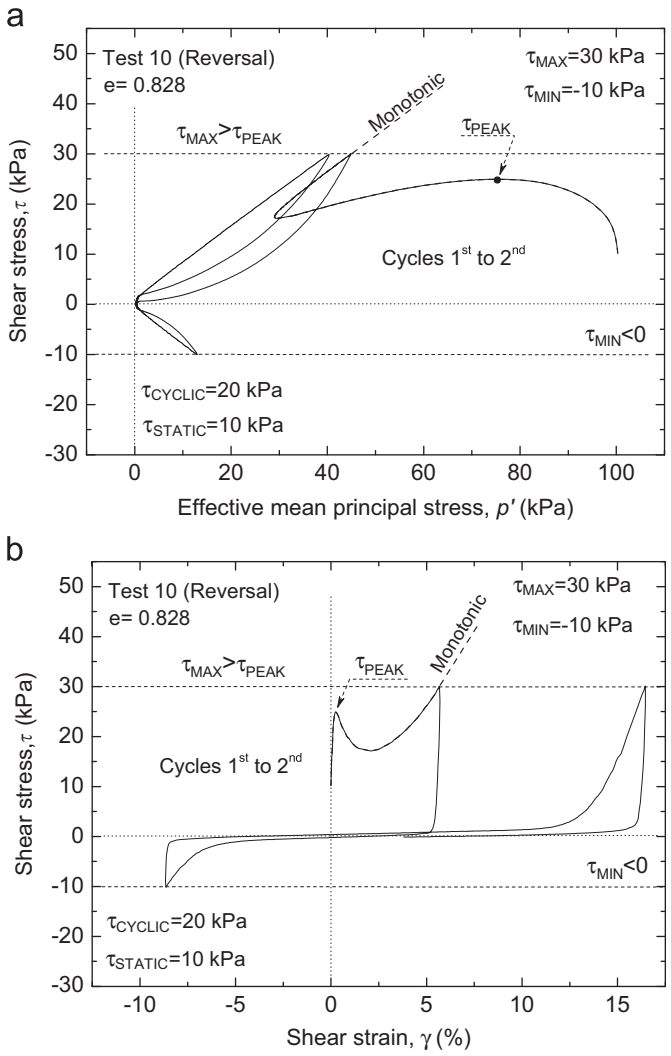

Fig. 9. Typical rapid flow liquefaction behavior.

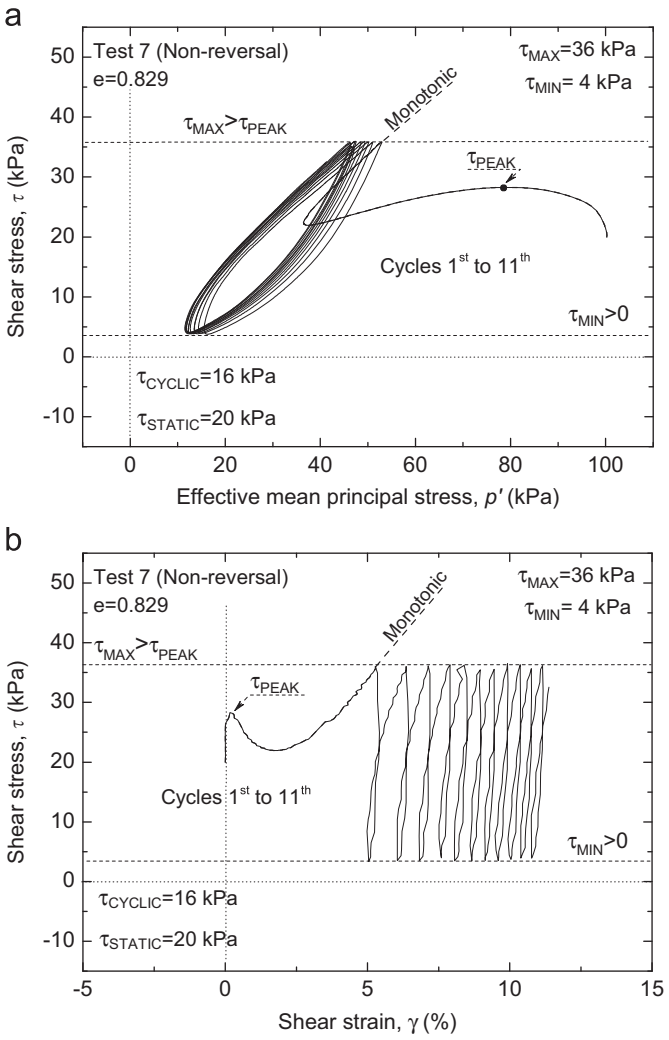

Fig. 10. Typical residual deformation failure behavior.

Residual deformation failure

In some tests, as typically shown in Fig. 10, the shear stress reached a maximum value which was higher than the transient peak stress during undrained monotonic loading ($\tau_{max} > \tau_{peak}$), as well as a positive minimum shear stress value ($\tau_{min} > 0$). Under these stress conditions (i.e., non-reversal stress), large deformations were achieved during cyclic loading, while liquefaction was not reached even after applying a hundred cycles. As a result, the residual deformation brought the sample to failure.

Resistance against cyclic strain accumulation

Usually, the resistance to liquefaction or cyclic strain accumulation is expressed by the cyclic stress ratio ($CSR = \tau_{cyclic}/p'_0$) required to develop a specific amount of deformation from the initial configuration of the specimen or during cyclic loading (i.e., single- or double-amplitude shear strain). However, in many cases, it can be seen that the cyclic stress ratio is not a sufficient single parameter for describing the effects of the initial static shear on the resistance to liquefaction or cyclic strain accumulation. To address this issue, the liquefaction resistance curves were described in this study in terms of both the cyclic stress ratio ($CSR = \tau_{cyclic}/p'_0$) and the static stress ratio ($SSR = \tau_{static}/p'_0$), as listed in Table 2.

Moreover, to describe the liquefaction resistance, the double-amplitude shear strain (γ_{DA}) and/or single-amplitude shear strain at the maximum shear stress state (γ_{SA} at $\tau = \tau_{max}$) are used. In this study, by applying the initial static shear, however, the stress conditions become non-symmetric with respect to the initial stress state, as schematically shown in Fig. 11. As a result, γ_{DA} is not well representative of the strain accumulation during cyclic loading. Therefore, in order to be consistent with previous studies, the resistance against liquefaction (or more strictly, the resistance to strain accumulation) was evaluated in terms of the number of cycles required to develop a specific amount of single-amplitude shear strain (γ_{SA}).

Figs. 12–14 show the number of cycles to achieve a single-amplitude shear strain of $\gamma_{SA} = 7.5\%$, $\gamma_{SA} = 20\%$ and $\gamma_{SA} = 50\%$, respectively.

Table 2
Resistance against strain accumulation and failure characteristics.

Test	*SSR*	*CSR*	$N_{7.5}$ ($\gamma_{SA}=7.5\%$)	N_{20} ($\gamma_{SA}=20\%$)	N_{50} ($\gamma_{SA}=50\%$)	Type of failure
1	0.00	0.16	35	38	48	CLQ
2	0.05	0.16	20	26	33	CLQ
3	0.10	0.16	10	13	20	CLQ
4	0.15	0.16	1.2	3.2	6.9	RFL
5	0.16	0.16	1.9	4.0	13	RFL
6	0.17	0.16	3.2	13	30	RSD
7	0.20	0.16	3.2	46	202	RSD
8	0.00	0.20	3.2	6.3	18	CLQ
9	0.05	0.20	2.2	4.4	14	CLQ
10	0.10	0.20	1.1	2.0	6.9	RFL
11	0.15	0.20	1.1	2.0	5.7	RFL
12	0.20	0.20	0.9	2.6	7.8	RFL
13	0.25	0.20	0.9	39	225	RSD

p'_0=initial effective mean principal stress (=100 kPa),
$SSR=\tau_{static}/p'_0$: static stress ratio, $CSR=\tau_{cyclic}/p'_0$: cyclic stress ratio,
CLQ: cyclic liquefaction, RFL: rapid flow liquefaction, RSD: residual deformation failure.

Fig. 12(b) shows that the number of cycles, $N_{7.5}$, to achieve a moderated strain level of $\gamma_{SA}=7.5\%$, which would correspond to a single-amplitude axial strain of $\varepsilon_a=5\%$ in undrained cyclic triaxial tests, decreases with an increase in SSR, except for the case of $CSR=0.16$, in which the $N_{7.5}$ value slightly increases to 3.2 at $SSR=0.16$–0.20 after achieving a minimum value of $N_{7.5}=1.2$ at $SSR=0.15$.

On the other hand, Fig. 13(b) reveals that the number of cycles, N_{20}, to achieve a large shear strain level of $\gamma_{SA}=20\%$ first decreases and then increases with an increase in *SSR*, irrespective of the level of *CSR*. It should be noted that the cyclic strain accumulation resistance shown in Fig. 13 is free from the effects of strain localization during undrained cyclic shearing, which may initiate at strain levels of about $\gamma_{SA}=23$–28%, as evaluated by Chiaro et al. (2011).

Finally, Fig. 14(b) shows that the number of cycles, N_{50}, to achieve an extremely large shear strain level of $\gamma_{SA}=50\%$, has the same characteristics as N_{20} defined at $\gamma_{SA}=20\%$, in the sense that they can either increase or decrease with an increase in *SSR*. However, these relationships between *CSR* or *SSR* and N_{50} should be taken only as reference data, since they are affected by strain localization (i.e., the formation of shear bands) during undrained torsional shear loading (Chiaro et al., 2011).

Thus, these test results show that the level of shear strain at which the resistance against strain accumulation is defined (i.e., moderate or large strain levels) plays an important role in the evaluation of the effect of the initial static shear on the strain accumulation resistance characteristics. In addition, the two-phase change in strain accumulation behavior (i.e., first a decrease and then an increase in strain accumulation resistance with initial static shear) can be associated with a three-phase change in failure behavior, namely, from cyclic liquefaction to rapid flow liquefaction to residual deformation failure.

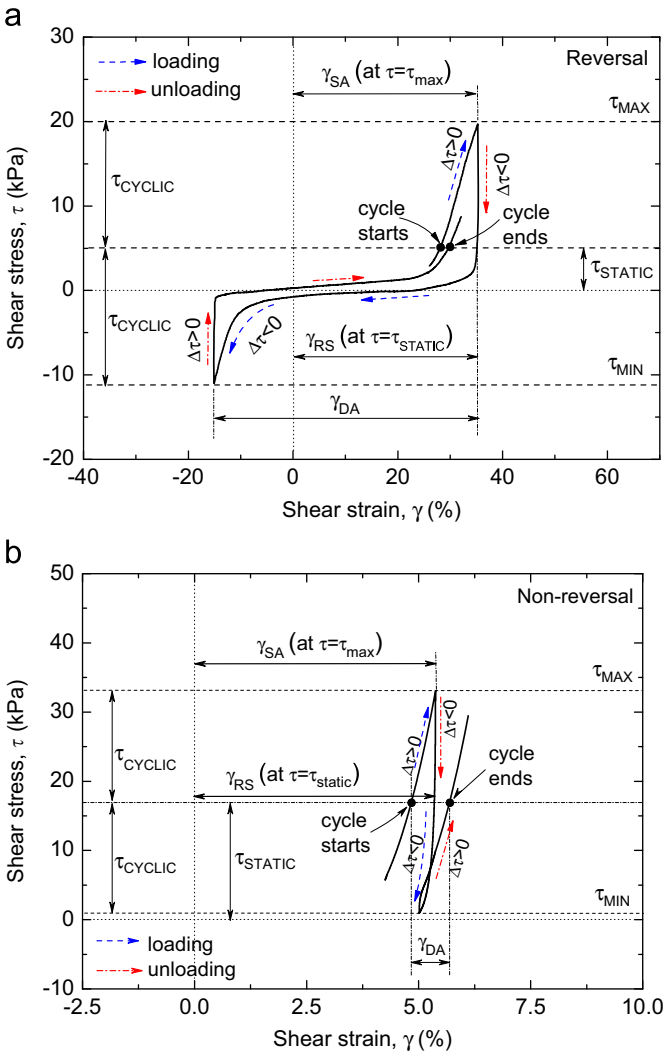

Fig. 11. Definition of shear strain components: (a) stress reversal and (b) non-reversal loading conditions.

Residual deformation development of sand with initial static shear

The value of γ_{SA}, defined at $\tau=\tau_{max}$, may be used to estimate the largest cyclic shear deformation of slopes during earthquakes. On the other hand, the residual deformation of slopes just after earthquakes can be estimated using the residual shear strain defined at a cyclic shear stress of zero (i.e., $\tau=\tau_{static}$) (Tatsuoka et al., 1982). However, in the current study, it is found that γ_{SA} and γ_{RS} almost coincide with each other (Fig. 11). Therefore, to examine the effects of the initial static shear on the residual deformation properties of saturated loose sand in undrained cyclic torsional shear tests, the residual shear strain was evaluated in terms of γ_{SA}. As already described previously, depending on the extent of τ_{static} and its combination with τ_{cyclic}, sand may undergo three different types of behavior, namely, cyclic liquefaction, rapid flow liquefaction and residual deformation failure. In Fig. 15, the modes of development of residual deformation

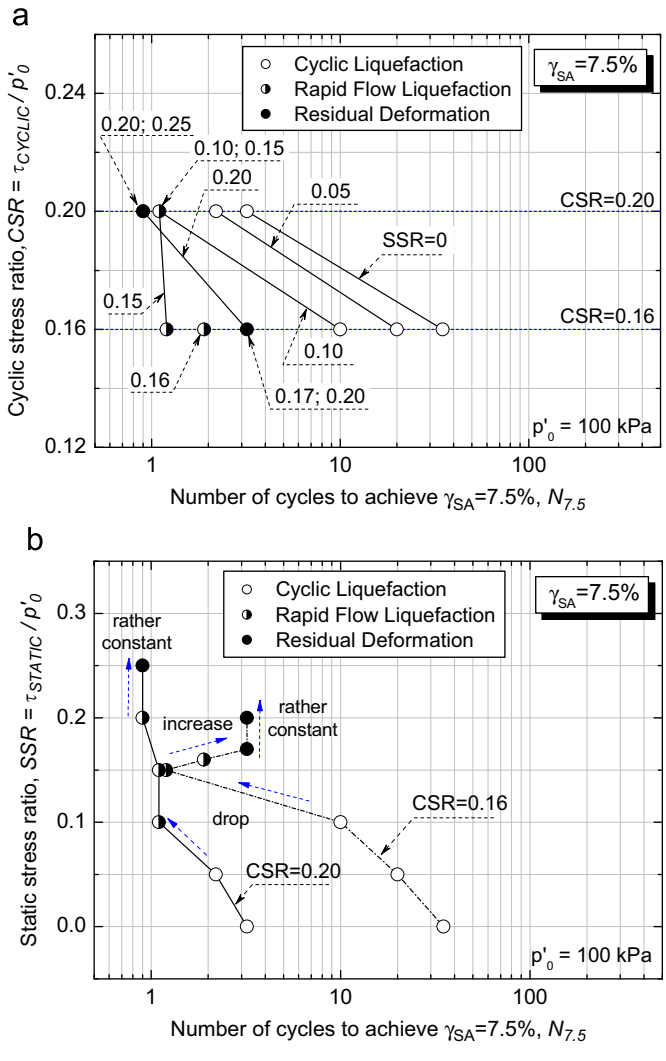

Fig. 12. Cyclic strain accumulation resistance for $\gamma_{SA}=7.5\%$: (a) *CSR*—number of cycles and (b) *SSR*—number of cycles.

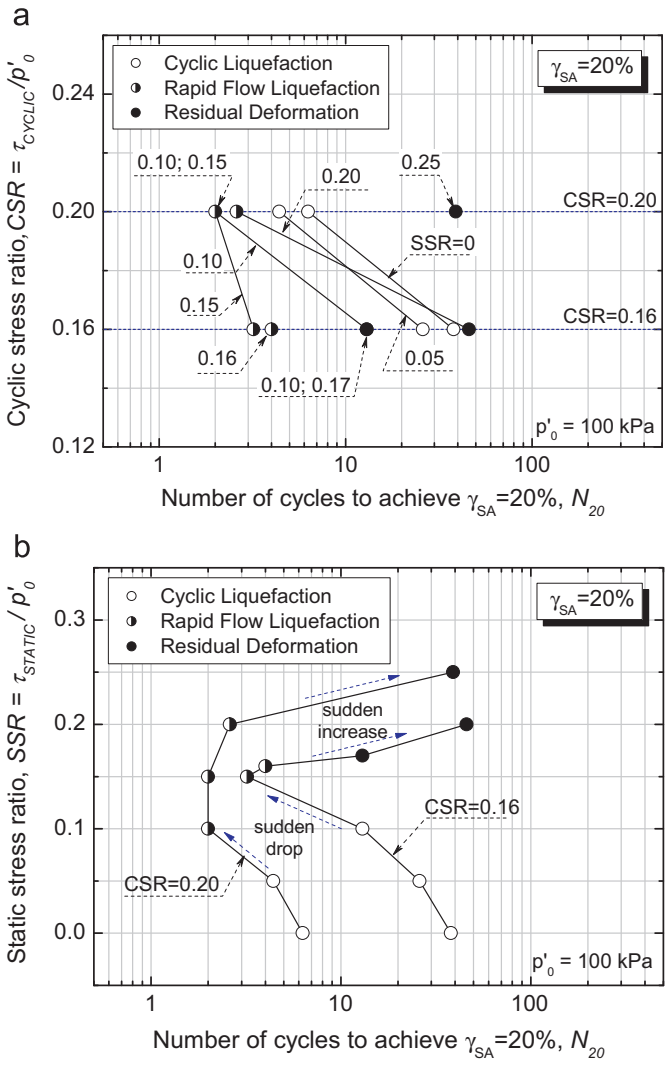

Fig. 13. Cyclic strain accumulation resistance for $\gamma_{SA}=20\%$: (a) *CSR*—number of cycles and (b) *SSR*—number of cycles.

associated with each of the observed types of sand behavior are reported.

In the case of either cyclic or rapid flow liquefaction behavior, Fig. 15(a) and (b), respectively, the higher the τ_{static}, the lower the number of cycles necessary to reach extremely large residual deformation. In addition, it can be observed that, following the achievement of the full liquefaction state ($p'=0$), large residual deformation developed in just 10–15 cycles. However, in the case of cyclic liquefaction behavior, the accumulation of large residual deformation may occur only after applying several cycles of loadings, while in the case of rapid flow liquefaction behavior, it occurs from the first cycle of loading. These test results clearly highlight the detrimental effect of τ_{static} in combination with τ_{cyclic}, which reduces the number of cycles up to the onset of liquefaction and signals the catastrophic development of extremely large residual deformation in the post-liquefaction stage.

On the other hand, as shown in Fig. 15(c), in the case of residual deformation behavior, since liquefaction did not occur, extremely large residual deformation may be achieved only by applying a large number of cycles.

Such tests results would be useful for investigating the failure mechanism that caused extremely large residual ground deformation in liquefied natural sand deposits during large-magnitude earthquakes (e.g., the 1964 Niigata Earthquake and the 1983 Nihonkai-Chubu Earthquake) that have occurred in Japan during the past decade, and to assess effective countermeasures to minimize the effects of the liquefaction-induced ground deformation of natural and artificial sloped grounds.

Discussion

Resistance to strain accumulation of sand based on torsional shear and triaxial tests with initial shear

Fig. 16 compares the strain accumulation resistance of loose saturated Toyoura sand obtained in this study by undrained cyclic torsional shear tests with that obtained by

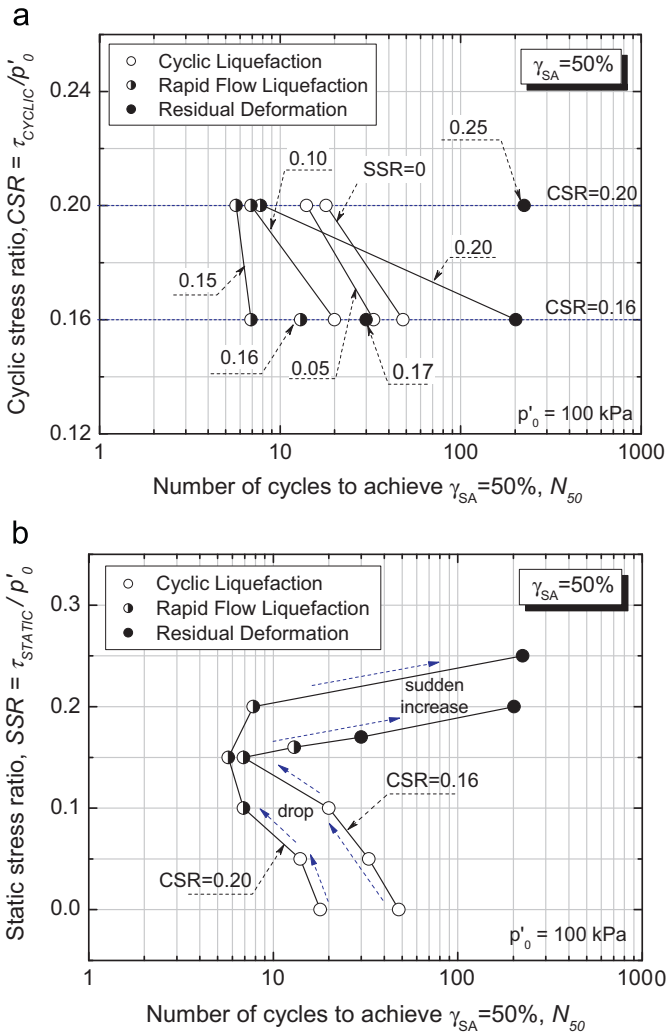

Fig. 14. Cyclic strain accumulation resistance for $\gamma_{SA}=50\%$: (a) *CSR*—number of cycles and (b) *SSR*—number of cycles.

Hyodo et al. (1994) by undrained cyclic triaxial tests, under similar initial conditions of relative density, confining pressure as well as applied static and cyclic shear stress. One can clearly see that the cyclic responses of sand, measured in terms of residual strain (i.e., $\gamma_{RS}=7.5\%$ for torsional tests and $\varepsilon_{RS}=5\%$ for triaxial tests), are in contrast to each other:

(a) Under torsional shear loading, the cyclic strain resistance firstly decreases with an increase in the initial static shear. As a result, the initial static shear has a detrimental effect on the liquefaction resistance of sand.
(b) On the contrary, under triaxial shear loading, an opposite trend was observed, where the cyclic strain resistance firstly increases with an increase in the initial static shear. Hence, in this case, the initial static shear seems to be favorable to the liquefaction resistance of sands. The possible reason is that the soil under cyclic triaxial shearing experiences both extension and compression behavior within a single cycle of loading. For low values of initial static shear, the extension behavior is predominant, which may cause the soil to liquefy quickly due to the effects of anisotropy. With an increase in the initial static shear on the triaxial compression side, the compression behavior predominates and the soil becomes more resistant to liquefaction. Therefore, the initial static shear has a beneficial effect on the liquefaction resistance of soil.

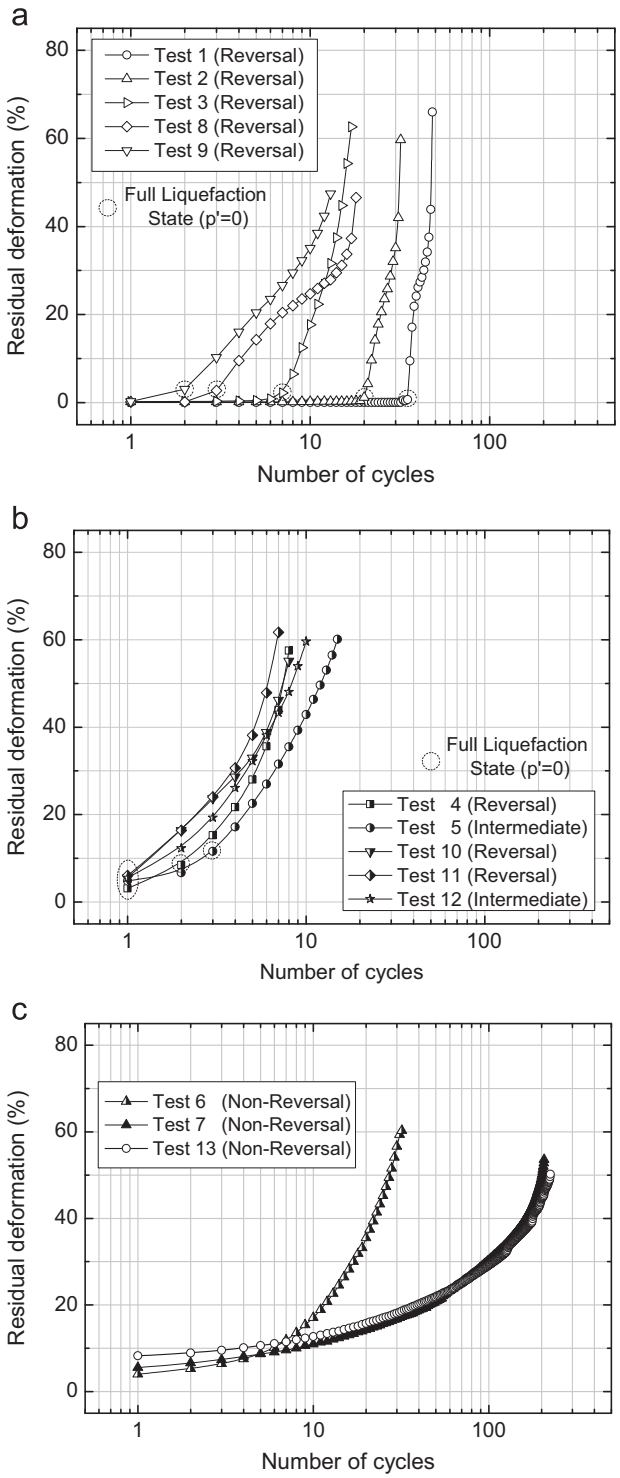

Fig. 15. Modes of development of residual deformation during undrained cyclic torsional loading.

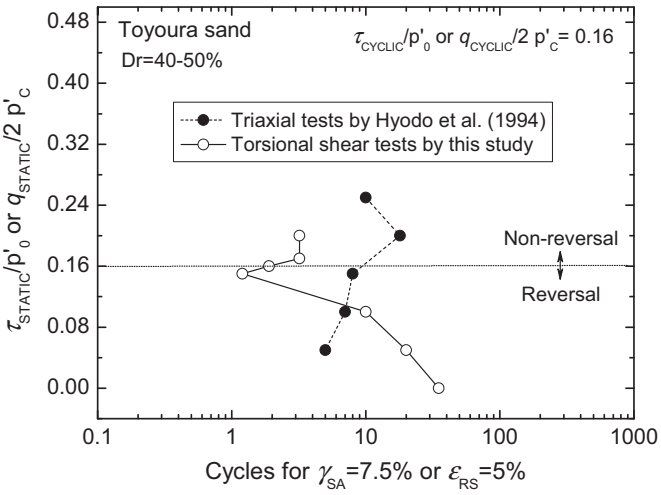

Fig. 16. Strain accumulation resistance of loose Toyoura sand by undrained cyclic torsional shear and triaxial tests with initial static shear.

Castro (1975) and Castro and Poulus (1977) concluded, based on triaxial test results, that strain accumulation resistance increases with an increase in initial static shear in a similar manner to that reported by Hyodo et al. (1994). However, by investigating the effect of axial extension during cyclic triaxial tests, they found that the larger deformation observed in the extension, with respect to compression for a given deviator stress, does not correspond to the field conditions; therefore, cyclic triaxial tests generally overestimate the cyclic deformation that may develop in the field due to liquefaction.

In summary, the evaluation of the effect of the initial static shear on the liquefaction resistance of sand is significantly affected by the testing method employed, and therefore, should be carefully addressed. To this regard, it is well recognized that simple shear tests can simulate field stress conditions expected during earthquakes more accurately than triaxial tests. Hence, torsional simple shear tests, as performed in this study, would be a useful tool for better understanding and evaluating the effect of the initial static shear on the cyclic undrained behavior of sand.

Conclusions

In order to evaluate the large deformation behavior and liquefaction properties of saturated sand with initial static shear stress, a series of undrained cyclic torsional tests was conducted at varying levels of initial static shear and cyclic shear stress amplitude. The following main conclusions were obtained.

(1) From the study of failure mechanisms, based on the difference in the effective stress paths and the modes of development of shear strain during both monotonic and cyclic loading behavior, the observed types of failure could be distinguished into three types, namely, cyclic liquefaction, rapid flow liquefaction and residual deformation failure. In the case of stress reversal and intermediate loadings, failure was associated with full liquefaction, followed by extremely large deformation in the post-liquefaction process. On the other hand, in the case of non-reversal loading, residual deformation brought the specimen to failure (i.e., the formation of spiral shear bands), although liquefaction did not occur.

(2) The test results show that the presence of initial static shear does not always lead to a monotonic change in the resistance to cyclic shear strain accumulation. It can either increase or decrease due to the increase in static shear, depending on the magnitude of the combined shear stress, the type of loading, the failure behavior and also the extent of the shear strain levels at which the resistance against strain accumulation is defined.

(3) The mechanisms of residual strain development depend on the failure behavior of the sand. In the case of cyclic liquefaction, the full liquefaction state ($p'=0$) followed by a sudden development of residual deformation was achieved after applying several cycles of loading. On the other hand, in the case of rapid flow liquefaction, during the first cycle, full liquefaction and shear strain of a few percent was achieved. In addition, in most of the tests, a residual shear strain exceeding 50% was reached in less than 10 cycles. On the contrary, in the case of residual deformation failure, extremely large deformation could be reached after applying a large number of cycles of loading, although liquefaction did not take place.

References

Alarcon-Guzman, A., Leonards, G.A., Chameau, J.L., 1988. Undrained monotonic and cyclic strength of sands. Journal of Geotechnical Engineering, ACSE 114 (10), 1089–1109.

Ampadu, S.K., Tatsuoka, F., 1993. Effects of setting method on the behavior of clays in triaxial compression from saturation to undrained shear. Soils and Foundations 33 (2), 14–34.

Castro, G., 1975. Liquefaction and cyclic mobility of saturated sand. Journal of the Geotechnical Engineering Division, ASCE 101 (GT6), 551–569.

Castro, G., Poulus, S.J., 1977. Factors affecting liquefaction and cyclic mobility. Journal of the Geotechnical Engineering Division, ASCE 103 (GT6), 501–551.

Chiaro, G., Kiyota, T., Koseki, J., 2011. Effects of initial static shear on shear strain localization characteristics of sand in undrained cyclic torsional shear tests. In: Proceedings of 8th International Conference on Urban Earthquake Engineering. Tokyo, Japan, pp. 531–536.

De Silva, L.I.N., Koseki, J., Sato, T., 2006. Effects of different pluviation techniques on deformation property of hollow cylinder sand specimens. In: Proceedings of the International Symposium on Geomechanics and Geotechnics of Particulate Media, Ube, Yamaguchi, Japan, pp. 29–33.

Hamada, M., O'Rourke, T.D., Yoshida, N., 1994. Liquefaction-induced large ground displacement. In: Performance of Ground and Soil Structures during Earthquakes, 13th ICSMFE, pp. 93–108.

Hyodo, M., Murata, H., Yasufuku, N., Fujii, T., 1991. Undrained cyclic shear strength and residual shear strain of saturated sand by cyclic triaxial tests. Soils and Foundations 31 (3), 60–76.

Hyodo, M., Tanimizu, H., Yasufuku, N., Murata, H., 1994. Undrained cyclic and monotonic triaxial behavior of saturated loose sand. Soils and Foundations 34 (1), 19–32.

Ishihara, K., Tatsuoka, F., Yasuda, S., 1975. Undrained deformation and liquefaction of sand under cyclic stresses. Soils and Foundations 15 (1), 29–44.

Kiyota, T., Sato, T., Koseki, J., Mohammad, A., 2008. Behavior of liquefied sands under extremely large strain levels in cyclic torsional shear tests. Soils and Foundations 48 (5), 727–739.

Koseki, J., Yoshida, T., Sato, T., 2005. Liquefaction properties of Toyoura sand in cyclic torsional shear tests under low confining stress. Soils and Foundations 45 (5), 103–113.

Koseki, J., Kiyota, T., Sato, T., Mohammad, A.M., 2007. Undrained cyclic torsional shear tests on sand up to extremely large strain levels. In: International Workshop on Earthquake Hazard and Mitigation, Guwahati, India, pp. 257–263.

Kramer, S.L., 1996. Geotechnical Earthquake Engineering. Prentice-Hall, New Jersey.

Lade, P.V., 1993. Initiation of static instability in the submarine Nerlerk berm. Canadian Geotechnical Journal 30 (6), 895–904.

Lee, K.L., Seed, H.B., 1967. Dynamic strength of anysotropically consolidated sand. Journal of the Soil Mechanics and Foundations Division, ASCE 93 (SM5), 169–190.

Seed, H.B., 1968. Land slides during earthquakes due to soil liquefaction. Journal of the Soil Mechanics and Foundations Division, ASCE 94 (SM5), 1055–1122.

Tatsuoka, F., Muramatsu, M., Sasaki, T., 1982. Cyclic undrained stress–strain behavior of dense sand by torsional simple shear test. Soils and Foundations 22 (2), 55–69.

Vaid, Y.P., Chern, J.C., 1983. Effects of static shear on resistance to liquefaction. Soils and Foundations 23 (1), 47–60.

Vaid, Y.P., Chern, J.C., 1985. Cyclic and monotonic undrained response of saturated sands. Advances in the Art of Testing Soils Under Cyclic Conditions, ACSE Convention, Detroit, USA, pp. 120–147.

Vaid, Y.P., Finn, W.D.L., 1979. Static shear and liquefaction potential. Journal of the Geotechnical Engineering Division, ASCE 105 (GT10), 1233–1246.

Verdugo, R., Ishihara, K., 1996. The steady state of sandy soils. Soils and Foundations 36 (2), 81–92.

Yang, J., Sze, Y., 2011. Cyclic behavior and resistance of saturated sand under non-symmetrical loading conditions. Geotechnique 61 (1), 59–73.

Yoshimi, Y., Oh-oka, H., 1975. Influence of degree of shear stress reversal on the liquefaction potential of saturated sand. Soils and Foundations 15 (3), 27–40.